NANO LETTERS

pubs.acs.org/NanoLett Letter

Fluorofoldamer-Based Salt- and Proton-Rejecting Artificial Water Channels for Ultrafast Water Transport

Jie Shen, Arundhati Roy, Himanshu Joshi, Laxmicharan Samineni, Ruijuan Ye, Yu-Ming Tu, Woochul Song, Matthew Skiles, Manish Kumar,* Aleksei Aksimentiev,* and Huaqiang Zeng*

Cite This: *Nano Lett.* 2022, 22, 4831−4838 Read Online

ACCESS | Metrics & More | Article Recommendations | Supporting Information

ABSTRACT: Here, we report on a novel class of fluorofoldamer-based artificial water channels (AWCs) that combines excellent water transport rate and selectivity with structural simplicity and robustness. Produced by a facile one-pot copolymerization reaction under mild conditions, the best-performing channel (AWC **1**) is an n-C_8H_{17}-decorated foldamer nanotube with an average channel length of 2.8 nm and a pore diameter of 5.2 Å. AWC **1** demonstrates an ultrafast water conduction rate of 1.4×10^{10} H_2O/s per channel, outperforming the archetypal biological water channel, aquaporin 1, while excluding salts (i.e., NaCl and KCl) and protons. Unique to this class of channels, the inwardly facing C(sp2)-F atoms being the most electronegative in the periodic table are proposed as being critical to enabling the ultrafast and superselective water transport properties by decreasing the channel's cavity and enhancing the channel wall smoothness via reducing intermolecular forces with water molecules or hydrated ions.

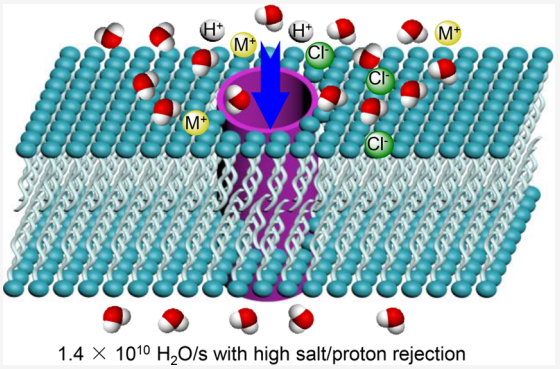

1.4 × 10^{10} H_2O/s with high salt/proton rejection

KEYWORDS: *Supramolecular chemistry, foldamer, artificial water channel, fluorine chemistry, water purification*

Scarcity of clean water is one critical challenge currently affecting over 4 billion people worldwide.[1,2] An important state-of-the-art technology for clean water production and wastewater reuse is reverse-osmosis (RO) membrane desalination.[3] The key to RO desalination is precise control over transient or fixed subnanometer scale passages, allowing water molecules to pass through the membrane while excluding other solutes like salt ions.[4]

In nature, living organisms regulate transmembrane water flow by membrane-embedded water channels, namely aquaporins (AQPs). AQPs facilitate superfast water translocation and completely reject salts and even protons.[5,6] For instance, AqpZ, isolated from *E. coli*, features a water transport rate of ∼6×10^9 H_2O/s.[7,8] The other type of AQPs, AQP1, present in specific human cells, can transport ∼1.1×10^{10} H_2O/s,[9] yet with remarkably high water to monovalent ion selectivity over 10^9. Integration of such water-permeating and salt-rejecting AQPs into polymer-based membranes represents an emerging approach for developing the next generation of water desalination and purification technology.[10−12] Nevertheless, AQPs usually suffer from high production costs, challenges with scalability, and questions about structural stability in abiotic environments,[13] making them less ideal for large-scale industrial applications.

Motivated by the superior performance of natural AQPs, researchers have expanded extensive effort in developing artificial water channels (AWCs) with simpler structures yet comparable or even exceeding water transport capabilities.[14−16] In 2007, Percec and co-workers reported the pioneering work in this field, wherein dendritic dipeptides were employed for the construction of AWCs in a lipid membrane.[17,18] Thereafter, various types of unimolecular or self-assembled AWCs have been designed and characterized including imidazole-quartet,[19−24] pillar[n]arenes,[25−28] aromatic macrocycles,[29] carbon nanotube porins (CNTPs),[30,31] porous organic cages,[32] helically folded polymeric nanotubes,[33−35] and hydrophilic hydroxyl assemblies.[36] The collective conclusion states that water transport efficiency and selectivity highly depend on the geometry and surface chemistry of the channel interior lumen, in which channel−water and water−water interactions occur, primarily via H-bonds.[9,34,35] However, concurrently achieving high single-channel water permeability and high transport selectivity (e.g., rejection of salts and protons) in a single AWC still remains a daunting task to date that has been addressed in only a few studies.[27,35]

Received: March 21, 2022
Revised: June 4, 2022
Published: June 8, 2022

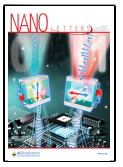

https://doi.org/10.1021/acs.nanolett.2c01137
Nano Lett. 2022, 22, 4831−4838

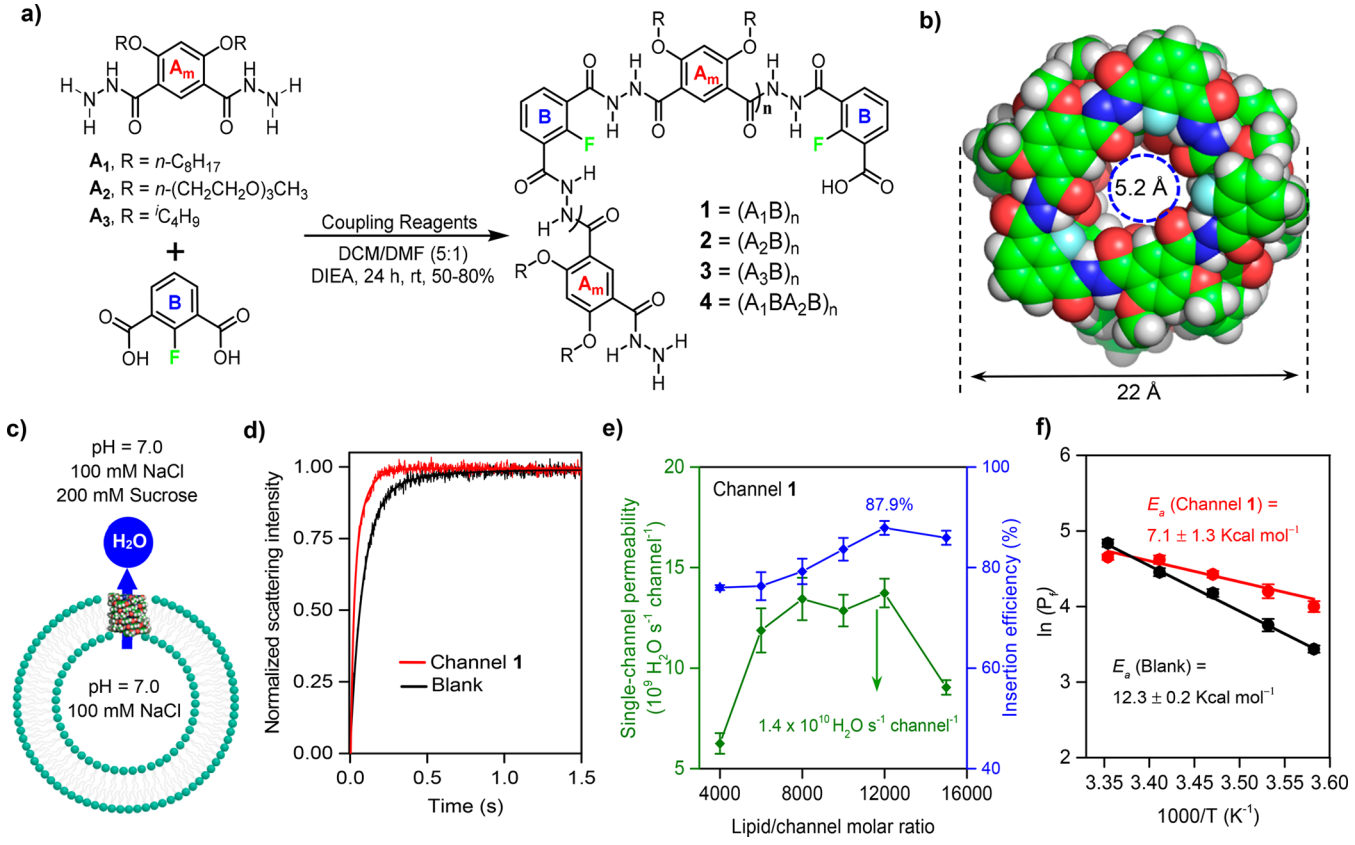

Figure 1. Molecular structures and water transport properties of fluorofoldamer-based AWCs at room temperature. (a) One-pot copolymerization mediated by amide coupling reagents. (b) Quantum mechanics-computed helically folded tubular structure for an octameric $(\mathbf{A_1B})_8$ oligomer at the HF/6-31G(d) level that gives rise to three **AB** units per helical turn; side chains are omitted for clarity. (c) Schematic illustration of LUV-based water permeability experiment in the presence of 200 mM sucrose as hypertonic solution. (d) Representative stopped-flow light scattering traces of blank DOPC LUV of ~120 nm in diameter and channel **1** reconstituted LUVs under the inwardly directed osmotic gradient. (e) Single channel water permeability and insertion efficiency for **1** at different lipid/channel molar ratios. (f) Arrhenius plots of the water permeability as a function of temperature for DOPC only and **1** for determining activation energies (E_a) averaged over three independent runs.

Here we report on such a high-performance salt- and proton-rejecting AWC system that has a 5.2 Å-diameter cavity and transports water at a rate better than AQP1, outperforming by greater than a factor of 4 all other hitherto known salt-rejecting AWCs, except for one very recent example.[35]

Molecular Design Incorporating Electron-Withdrawing F Atoms. Although the lone pair donation from the most electronegative fluorine is significantly suppressed, making it a poor H-bond acceptor,[37] early studies have established the ability of C(*sp*2)-F to form weak intramolecular H-bonds in foldamer structures.[38,39] Further, electron-withdrawing fluorine atoms may differ considerably from other H-bond-forming groups in determining the channel construct and guest (water, ion, etc.) binding behaviors[40] by decreasing the interior pore size and enhancing channel wall smoothness via reducing intermolecular host−guest H-bond interactions with water molecules or coordination bonds with cations, etc. With these points in mind, we decided to explore fluorofoldamer-based polymeric hollow channels of **AB** type (Figure 1a), having inward-facing fluorine atoms decorating the channel lumen, as possible AWCs.

AWC 1 Exhibits the Best Water Transport Performance. Screening a matrix of combinatorically produced AWCs culminated in the best performing AWC, water channel **1** (Figure 1a and Table S1). **1** is found to conduct water at an ultrafast rate of 1.4×10^{10} H_2O/s across the membrane, a value that is about two-times higher than its methoxy-containing analogous channel **1-OMe** (see later discussions). Further, **1** also demonstrates near-perfect salt (NaCl and KCl) and proton rejection, making it an excellent replacement of natural AQPs for possible industrial uses in fabricating a next-generation AWC-based RO membrane for seawater desalination or for use in therapeutics.[27]

AWC **1** was synthesized by following a reported protocol.[41] Briefly, a one-pot copolymerization reaction between diamine $\mathbf{A_1}$ and fluoro-containing diacid **B** using HBTU as the coupling reagent readily produced an off-white powdery product **1** with ~80% isolated yield (Figure 1a). Apart from extensive $\pi-\pi$ stacking, intramolecular H-bonds (R−O···H−N, C=O···H−N, and C(*sp*2)-F···H−N) are also expected to stabilize the polymeric product in a helically folded configuration.[42] Quantum mechanics computation of the pore scaffold (e.g., an octameric molecule $(\mathbf{A_1B})_8$, Figure 1B) was performed at the HF/6-31G(d) level that has consistently yielded accurate structural predictions for intramolecularly H-bonded foldamers.[43−45] Such computation shows that the optimized structure exhibits expected helical tubular structure, having three **AB** repeating units per helical turn (3.4 Å in helical pitch) and, after subtracting the van der Waals radii of the interior atoms, a pore diameter of ~5.2 Å, which is larger than a water molecule (2.8 Å) but smaller than first-shell hydrated Na^+ ions.

https://doi.org/10.1021/acs.nanolett.2c01137
Nano Lett. 2022, 22, 4831−4838

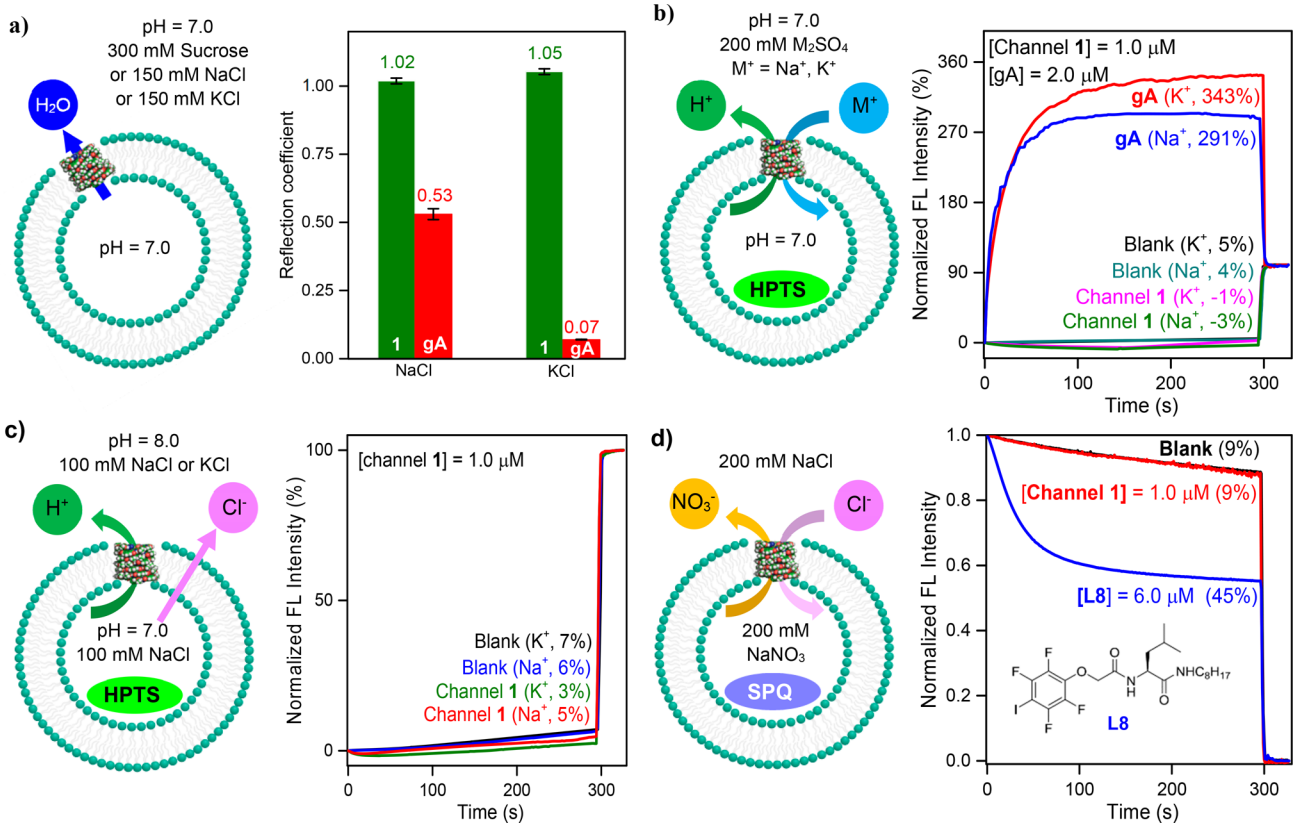

Figure 2. Ion exclusion properties of channel **1** at room temperature. (a) Reflection coefficients calculated from water permeabilities under three types of hypertonic conditions, suggesting high and low salt rejections by **1** and gA, respectively. (b) pH-sensitive HPTS-based LUV assays under high ionic concentration gradients, confirming that **1** does not transport both Na^+ and K^+ cations. (c) HPTS-based LUV assays under a proton gradient, pointing to an incapability of **1** in transporting protons. (d) Chloride-sensitive SPQ assay, demonstrating that **1** does not transport anions.

The average molecular weight of **1** was measured to be 13.9 kDa using gel permeation chromatography (GPC), which is consistent with a molecular weight of 15.4 kDa determined using the NMR-based method (Scheme S3, Figure S1, and Table S2). Using the simulated pore structure as the guide (three **AB** units per helical turn, MW of **AB** unit = 616.7 Da; see Figure 1b and Table S1), **1** contains 25 **AB** units on average, measuring at 2.8 nm in average nanotubular length, dimensionally comparable to the thickness of typical lipid bilayer membranes (e.g., 2.7 nm for DOPC).[46] In addition, **1** also displays a characteristic mass pattern with a repeating unit of 617 Da in the MALDI-TOF spectrum (Figure S2).

The stopped flow light-scattering method was employed to quantify the water transport efficiency, using large unilamellar vesicle (LUVs, 120 nm diameter, Figure 1c) with channel **1** preinserted in the LUV wall.[25,26] Under the shrinkage mode, LUVs were exposed to hypertonic buffer solution containing 200 mM sucrose. The time-dependent light-scattering intensities were captured and analyzed (Figure 1d), from which the water transport rate was determined. As shown in Figure 1e, water permeability of **1** was largely independent of the lipid to channel molar ratio (mLCR), and the profile peaked at 12 000:1 (~12 channel molecules per LUV), giving water permeability P_W of $(41.2 \pm 2.1) \times 10^{-14}$ cm^3/s. With a channel insertion efficiency of 87.9% at this mLCR (Table S3), water permeability translates into a single-channel water transport rate of $(1.4 \pm 0.07) \times 10^{10}$ H_2O/s, which becomes 0.78×10^{10} H_2O/s using the new equation for P_f correction.[47]

The temperature-dependent water permeability of **1** were measured from 6 to 25 °C, from which its activation energy E_a is calculated as 7.1 ± 1.2 kcal mol^{-1} using the Arrhenius equation (Figure 1f). It is higher than that of the AQPs (~5 kcal mol^{-1}) but much lower than that from the blank DOPC LUV (12.3 ± 0.2 kcal mol^{-1}). In view of the superior water conduction rate of **1** compared to AQPs, we assume that low activation energy might not be a necessary feature for highly permeable AWCs, likely because the transport mechanisms differ from that of AQPs in nature, as proposed before.[34,35]

Impact of Channel Length on Water Permeability. Following identical synthetic protocols,[41] other amide coupling reagents (HATU, BOP, and TBTU) produce the same $\mathbf{A_1B}$ type channels with NMR-derived molecular weights of 20.1, 19.9, and 13.1 kDa (Table S1) that correspond to channel lengths of 4.0, 4.0, and 2.6 nm, respectively. As summarized in Figure S3, their water transport rates were all found to be lower than AWC **1** (MW = 13.9 kDa, 2.8 nm). More specifically, at the mLCR of 12 000:1 and compared to **1** of 2.8 nm (P_w = 41.2×10^{-14} cm^3/s), $\mathbf{A_1B}$ type channels produced using HATU (4.0 nm), BOP (4.0 nm), and TBTU (2.6 nm) show much lower P_W values of 21.9×10^{-14}, 22.0×10^{-14}, and 32.4×10^{-14} cm^3/s, respectively.

Impact of Side Chain Type on Water Permeability. To examine the impact of channel side chains on water transport property, diamines $\mathbf{A_2}$ and $\mathbf{A_3}$ were also employed in the HBTU-facilitated copolymerization reaction. Their corresponding products $(\mathbf{A_2B})_n$ and $(\mathbf{A_3B})_n$ were named AWCs **2** and **3**, respectively. Monomers $\mathbf{A_1}$ and $\mathbf{A_2}$ were further

https://doi.org/10.1021/acs.nanolett.2c01137
Nano Lett. 2022, 22, 4831−4838

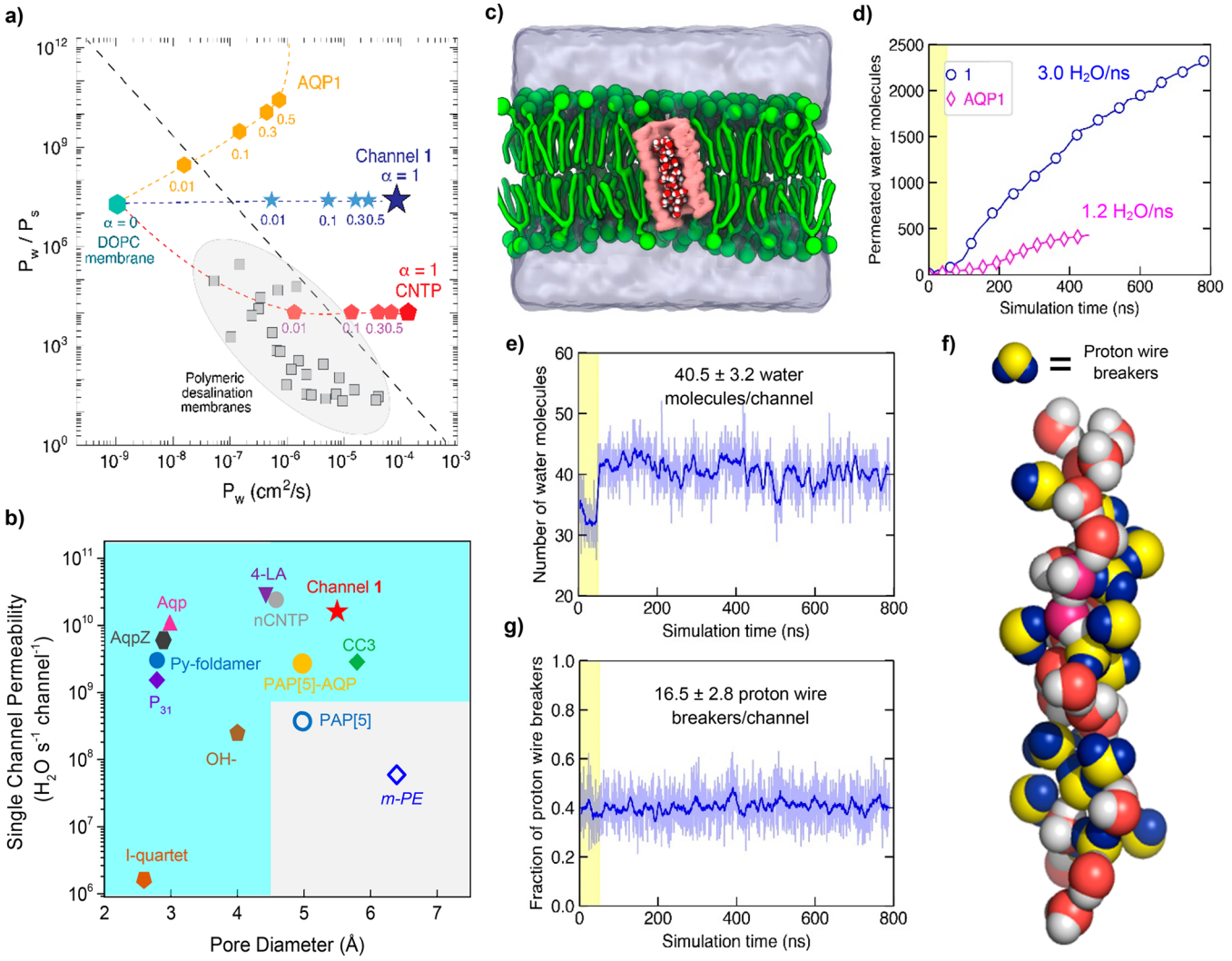

Figure 3. Ion exclusion and water transport properties of **1**, validated using MD simulations, point to its promise as a component of AWC-based desalination membranes. (a) Water-to-salt permselectivity values of **1**, some representative water channels, and current polymeric desalination membranes. CNTPs have pore diameter of ~0.47 nm.[55] The α values refer to the fractional membrane volume occupied by water channels (e.g., α = 0.5 represents the half membrane volume that comprises **1**. Dashed line corresponds to upper bound limit in permeability−selectivity value for the current polymer desalination membranes.[11,50] (b) Single-channel water conduction rate and channel pore diameter of natural AQPs (AqpZ[7,8] and AQP1[9,56]) and AWC systems including nCNTP,[31] CC3,[32] PAP[5]-AQP,[27] **4-LA**,[35,41] Py-foldamer,[34] $\mathbf{P_{31}}$,[33] OH-Channel,[36] I-quartet,[20] PAP[5],[26] and *m*-PE.[29] Except for nonselective nCNTP, those in the light blue shaded region demonstrate salt-rejecting ability, whereas those in the gray region are ion-conductive. (c) Representative snapshot of water-containing channel **1**, having 25 **AB** units and height of 2.8 nm, embedded in POPC membrane and solvated in 1 M aqueous solution of NaCl. (d) MD-derived water transport rates for **1** and AQP1. The channels were positionally restrained for the first 48 ns (highlighted region) of each MD trajectory. (e) Number of water molecules inside the channel, with a mean of 40.5 water molecules. (f) Fraction of proton wire breakers inside the channel, with a mean of 40.7% (16.5 water molecules per channel). (g) Water cluster consisting of 40 water molecules out of which 17 serve as proton wire breakers, preventing proton transport via the Grotthuss mechanism.

premixed in 1:1 ratio and then stoichiometrically reacted with **B** to produce mixed copolymers $(\mathbf{A_1BA_2B})_n$ (e.g., AWC **4**). From their NMR-derived molecular weights (Table S2), the channel tubular lengths can be estimated to be 3.1, 2.9, and 4.1 nm for **2**, **3**, and **4**, respectively. At the mLCR of 12 000:1, **2**−**4** show much lower P_W values of 2.8 × 10^{-14}, 20.2 × 10^{-14}, and 29.4 × 10^{-14} cm^3/s, respectively. The comparative data indicate the importance of side chain lipophilicity on water transport efficiency, and clearly the linear *n*-C_8H_{17} represents the best performer.

High Salt and Proton Rejection Capacity of AWC 1. One major challenge for AWCs in mimicking AQP performance is to achieve complete rejection of salts and protons. To this end, we first compared the osmotic water permeability (P_f in cm/s) values of **1** under three hypertonic conditions (300 mM sucrose, 150 mM NaCl, or 150 mM KCl, Figure 2a). Since large sucrose molecules are not able to permeate through AWC **1**, the reflection coefficient, defined as P_f(MCl)/P_f(sucrose) where M^+ = Na^+ or K^+, was used to approximately gauge the transport of salt ions. The well-established dimeric water- and cation-transporting channel gramicidin A (gA) was employed as the positive control, which showed expected reflection coefficients of 0.53 ± 0.02 and 0.07 ± 0.001 for NaCl and KCl, arising from its high permeability to both Na^+ and K^+ ions. In contrast, the reflection coefficients of **1** were calculated to be 1.02 ± 0.01 for Na^+ and 1.05 ± 0.01 for K^+ at

https://doi.org/10.1021/acs.nanolett.2c01137
Nano Lett. 2022, 22, 4831−4838

12 000:1 mLCR, confirming the inability of **1** to transport either cation across the membrane and its near-perfect salt rejection property.[20]

The rejection of Na^+ and K^+ cations was further validated by the fluorescence-based HPTS assay, with pH-sensitive HPTS dye molecules entrapped in the LUVs (Figure 2b). The intravesicular region is set pH 7, whereas the extravesicular environment is maintained at the same pH but with 200 mM M_2SO_4 (M = Na or K). Under this high salt gradient, H^+/M^+ antiport will increase the intravesicular pH and hence enhance the HPTS fluorescence intensity. As shown in Figure 2b, **1** at 1 μM was found nonresponsive toward Na^+ or K^+ gradient, affirming the impermeability of neither cation through **1**. However, gA at 1 μM efficiently transports Na^+ (291%) and K^+ (343%) cations. Such observation is in excellent agreement with the reflection coefficient results described earlier, both confirming the inability of **1** to transport cations.

The anion transport ability of **1** was examined by using Cl^--sensitive SPQ dye molecules entrapped in LUVs (Figure 2d). As expected, **1** at 1 μM displayed similar SPQ quenching as background (9%), whereas the chloride transporter **L8**[48] at 6 μM (corresponding to 1 μM channel concentration) displayed a significant decrease (45%) in the SPQ fluorescence intensity. In another set of LUV-based experiments where the intravesicular region has 100 mM NaCl at pH 7 and extravesicular region has 67 mM Na_2SO_4 at pH 8 (Figure S5), gA (cation channel, 1 μM), FCCP (proton carrier, 1 μM), and **L8** (anion channel, 1.3 μM) induce HPTS fluorescence increases of 56%, 22%, and 138%, respectively. In sharp contrast, **1** at 1 μM does not cause any fluorescence change.

Proton translocation was probed using the pH gradient set across the membrane (Figure 2c). If **1** is able to transport protons, the proton efflux will induce significant pH increase in the intravesicular region and dramatic change in HPTS fluorescence intensity. Experimentally, no fluorescence change was observed after the addition of **1** (1 μM), suggesting negligible transport of protons. Using a conservative approach (see the Supporting section "Estimation of Proton Transport Rate"), the proton transport rate of **1** is estimated to be less than 0.25 proton/s.

The same set of data seen in Figure 2c also can be used to establish the inability of **1** to transport cations. This is because if **1** can transport cations, the charge neutralization will require passive influx of protons, leading to enhanced HPTS fluorescence intensity. Indeed, we did not observe any fluorescence change upon addition of **1** (1 μM), suggesting negligible transport of cations including Na^+ and K^+.

Stopped-flow fluorescence analysis was further applied to quantitatively measure chloride permeability through DOPC membrane in the absence and presence of **1** (Figure S6).[35,49] On the basis of the determined single-channel Cl^- permeability P_{Cl} of $(1.7 \pm 07) \times 10^{-20}$ cm^3/s, the water-to-Cl^- permselectivity (e.g., P_W/P_{Cl}) for **1** was calculated to be $(2.5 \pm 1.2) \times 10^7$. Since NaCl permeability is limited by the Na^+ ions in actual desalination processes,[49] 2.5×10^7 represents a conservative estimate of the water-to-NaCl permselectivity, exceeding the permeability-selective trade-off trendline of current desalination membranes[11,50] by a factor of $\sim 10^2$ (Figure 3a). This signifies good potential for developing novel AWC-based desalination membrane that incorporates or is made of **1**.

Comparison with Two High-Performance AWCs. As summarized in Figure 3b, currently there are only two water-transporting systems with higher water conduction rates than both AQP1 (1.1×10^{10} H_2O/s)[9] and AWC **1** (1.4×10^{10} H_2O/s), that is, the relatively low selectivity CNT porin (2.3×10^{10} H_2O/s)[31] and the highly selective AWC **4-LA** (2.7×10^{10} H_2O/s).[35] While the water-transporting CNT porin also conducts ions and protons,[31] channel **4-LA** requires additional lipid anchors (**LA**) installed at the helical ends to orient the channel's alignment to achieve the ultrafast water conduction.[35] Without such **LA** modifications, its water transport rate drastically drops by 75% to $\sim 0.6 \times 10^{10}$ H_2O/s,[35] a value that is ~43% of the capacity of **1**. Further, it is possible that the **LA**-enhanced water transport property might deteriorate over time or be altered by the complex environment of a water purification membrane. All these make both CNTP and **4-LA** potentially less competitive for fabricating practical AWC-based biomimetic water purification membranes than **1**.[12,51] Also in this regard, **1** perhaps represents the best artificial water channel ever reported in terms of simplicity of design, structural robustness, facile synthesis, and water transport properties.

Critical Roles Played by Fluorine Atoms. To demonstrate the crucial role of C(*sp*2)-F moieties in determining the water transport property, we compared **1** with the recently reported analogous channel denoted as **1-OMe** of 3.0 nm in height, which differs from **1** in that **1-OMe** contains methoxy groups in the positions of the F atoms of **1**.[35] As a result of bulky hydrophobic methyl groups helically arranged around the pore interior of **1-OMe**, its helical backbone is slightly less curved than that of **1** having its pore surface decorated by F atoms. Consequently, the pore diameter of **1-OMe** is enlarged to 6.5 Å across (vs 5.2 Å across for **1**). Under the identical conditions, the water transport rate of **1-OMe** was determined at $\sim 5 \times 10^9$ H_2O/s,[35] which is 36% of that of **1**. Furthermore, unlike **1** with excellent ion-rejection capability, **1-OMe** was permeable to anions.[41] Therefore, we speculate that the superior water transport properties of **1** should arise from a collection of influencing factors induced by the inward-facing C(*sp*2)-F moieties including the smaller atomic size, weak H-bond acceptor ability, dipolar bond characteristics, and good hydrophobicity.

Molecular Dynamics Simulation. To provide a molecular-level explanation of transmembrane water transport through **1** embedded in POPC lipid bilayer membrane, we performed 800 ns long all-atom molecular dynamics (MD) simulations (Figure 3c and Supporting Video 1). To maintain a QM-derived diameter of **1**, we used the *RMSD colvar* module of NAMD during the course of MD simulation. As the simulation begins, water molecules rapidly start permeating across the lipid bilayer through **1** (Figure 3d). Starting from the initial upright conformation, the channel explores an ensemble of tilted conformations (possible experimental structures) in the membrane during the course of the MD simulation. A linear fit to the water permeation versus simulation time (excluding first 200 ns) yields a permeation rate of ~3 water molecules/ns for **1**, which is higher than 1.2 water molecules/ns for AQP1. At any given instant of time, a water cluster residing inside the channel typically has 30−50 water molecules, with a mean of 40.5 water molecules (Figure 3e). Among them, 40.7% or 16.5 water molecules are considered as proton wire breakers (Figure 3f), which were described and defined in our recent study.[35] Interacting with the neighboring water molecules via zero or just one H-bond, or two H-bonds solely via only O atoms or only H atoms

https://doi.org/10.1021/acs.nanolett.2c01137
Nano Lett. 2022, 22, 4831−4838

(Figure 3g), these breakers prevent formation of a continuously H-bonded channel-spanning water chain through which protons hop via the Grotthuss mechanism. Interestingly, the breaker type involving the formation of two H-bonds with the adjacent water molecules using only H atoms is also observed in the NPA motif of AQPs.[52] The existence of these proton wire breakers accounts for low proton permeability of **1**.

Because of the narrow pore, each water molecule forms 1.94 H-bonds with other water molecules inside the channel (Figure S9a,b) and 0.79 H-bonds with the channel wall (Figure S9c), leading to a total of 2.73 H-bonds per water molecule. Taking 4 H-bonds per water molecule ($E_{H\text{-}bond}$ = 5.1 kcal/mol) in bulk water,[53,54] the activation energy for water entry into **1** can be estimated to be 6.5 kcal/mol, which is consistent with the experimentally determined value of 7.1 kcal/mol (Figure 1f). The fact that **1** has a higher activation energy but transports water faster than AQP1 may be attributed to its larger pore diameter of 5.2 Å versus ∼2.8 Å opening in the central channel of AQP1 as well as more than one water wire molecule occupying the pore lumen that differs from the single file transport seen in AQP1.[35]

In summary, we have demonstrated ultrahigh water transport efficiency and excellent selectivity of a novel class of fluorofoldamer-based artificial water channels. Produced by facile one-pot copolymerization reaction with good yields, the best-performing water channel **1** of 2.8 nm in average channel length shows a remarkable water conduction rate of 1.4×10^{10} H_2O/s and near-perfect rejection of salt ions (Na^+, K^+, Cl^-) and protons. This work uncovers the positive effects of introducing C(*sp*2)-F moieties on the inner rim of foldamer-based water channel pores, providing a new dimension of channel design principles. This, we believe, will stimulate further development toward the next generation of membrane technologies for water desalination, nanofiltration, and medical dialysis applications.

■ ASSOCIATED CONTENT

Supporting Information

The Supporting Information is available free of charge at https://pubs.acs.org/doi/10.1021/acs.nanolett.2c01137.

Synthetic procedures, GPC- and NMR-derived molecular weights, MALDI-TOF spectrum, water transport characterization method, additional ion transport data, molecular modeling, ^{1}H and ^{13}C NMR (PDF)

Transmembrane water transport through **1** embedded in POPC lipid bilayer membrane MD simulation (MP4)

■ AUTHOR INFORMATION

Corresponding Authors

Manish Kumar − *McKetta Department of Chemical Engineering, The University of Texas at Austin, Austin, Texas 78712, United States; Department of Civil, Architectural and Environmental Engineering, The University of Texas at Austin, Austin, Texas 78712, United States;* Email: manish.kumar@utexas.edu

Aleksei Aksimentiev − *Department of Physics and Beckman Institute for Advanced Science and Technology, University of Illinois at Urbana−Champaign, Urbana, Illinois 61801, United States;* orcid.org/0000-0002-6042-8442; Email: aksiment@illinois.edu

Huaqiang Zeng − *School of Chemistry and Chemical Engineering, Northwestern Polytechnical University, Xi'an, Shaanxi 710072, China;* orcid.org/0000-0002-8246-2000; Email: hqzeng@fzu.edu.cn

Authors

Jie Shen − *School of Chemistry and Chemical Engineering, Northwestern Polytechnical University, Xi'an, Shaanxi 710072, China;* orcid.org/0000-0003-1768-8748

Arundhati Roy − *Department of Pharmacy, Ludwig Maximilian University, Munich 81377, Germany*

Himanshu Joshi − *Department of Physics and Beckman Institute for Advanced Science and Technology, University of Illinois at Urbana−Champaign, Urbana, Illinois 61801, United States*

Laxmicharan Samineni − *McKetta Department of Chemical Engineering, The University of Texas at Austin, Austin, Texas 78712, United States*

Ruijuan Ye − *School of Chemistry and Chemical Engineering, Northwestern Polytechnical University, Xi'an, Shaanxi 710072, China;* orcid.org/0000-0002-4188-8830

Yu-Ming Tu − *McKetta Department of Chemical Engineering, The University of Texas at Austin, Austin, Texas 78712, United States;* orcid.org/0000-0002-2007-5005

Woochul Song − *McKetta Department of Chemical Engineering, The University of Texas at Austin, Austin, Texas 78712, United States;* orcid.org/0000-0001-6490-842X

Matthew Skiles − *Department of Civil, Architectural and Environmental Engineering, The University of Texas at Austin, Austin, Texas 78712, United States*

Complete contact information is available at: https://pubs.acs.org/10.1021/acs.nanolett.2c01137

Notes

The authors declare no competing financial interest.

■ ACKNOWLEDGMENTS

This work was supported by the National Science Foundation (USA) under Grant No. DMR-1827346 and the National Institutes of Health under Grant No. P41-GM104601. The work in MK lab was supported by the US National Science Foundation under Grant Nos. CBET 1946392 and CBET 1952295. Supercomputer time was provided through the Leadership Resource Allocation MCB20012 on Frontera of the Texas Advanced Computing Center and the Extreme Science and Engineering Discovery Environment (XSEDE) Allocation No. MCA05S028.

■ REFERENCES

(1) Mekonnen, M. M.; Hoekstra, A. Y. Four billion people facing severe water scarcity. *Sci. Adv.* **2016**, *2*, e1500323.

(2) Hoekstra, A. Y.; Wiedmann, T. O. Humanity's unsustainable environmental footprint. *Science* **2014**, *344*, 1114.

(3) Imbrogno, J.; Belfort, G. Membrane Desalination: Where Are We, and What Can We Learn from Fundamentals? *Annu. Rev. Chem. Biomol. Eng.* **2016**, *7*, 29−64.

(4) Culp, T. E.; Khara, B.; Brickey, K. P.; Geitner, M.; Zimudzi, T. J.; Wilbur, J. D.; Jons, S. D.; Roy, A.; Paul, M.; Ganapathysubramanian, B.; Zydney, A. L.; Kumar, M.; Gomez, E. D. Nanoscale control of internal inhomogeneity enhances water transport in desalination membranes. *Science* **2021**, *371*, 72−75.

(5) Murata, K.; Mitsuoka, K.; Hirai, T.; Walz, T.; Agre, P.; Heymann, J. B.; Engel, A.; Fujiyoshi, Y. Structural determinants of water permeation through aquaporin-1. *Nature* **2000**, *407*, 599−605.

(6) Tajkhorshid, E.; Nollert, P.; Jensen, M. Ø.; Miercke, L. J. W.; O'Connell, J.; Stroud, R. M.; Schulten, K. Control of the Selectivity of

the Aquaporin Water Channel Family by Global Orientational Tuning. *Science* **2002**, *296*, 525.
(7) Borgnia, M. J.; Kozono, D.; Calamita, G.; Maloney, P. C.; Agre, P. Functional reconstitution and characterization of AqpZ, the E. coli water channel protein11Edited by W., Baumeister. *J. Mol. Biol.* **1999**, *291*, 1169−1179.
(8) Horner, A.; Siligan, C.; Cornean, A.; Pohl, P. Positively charged residues at the channel mouth boost single-file water flow. *Faraday Discuss.* **2018**, *209*, 55−65.
(9) Horner, A.; Zocher, F.; Preiner, J.; Ollinger, N.; Siligan, C.; Akimov, S. A.; Pohl, P. The mobility of single-file water molecules is governed by the number of H-bonds they may form with channel-lining residues. *Sci. Adv.* **2015**, *1*, e1400083.
(10) Kumar, M.; Grzelakowski, M.; Zilles, J.; Clark, M.; Meier, W. Highly permeable polymeric membranes based on the incorporation of the functional water channel protein Aquaporin Z. *Proc. Natl. Acad. Sci. U.S.A.* **2007**, *104*, 20719−20724.
(11) Park, H. B.; Kamcev, J.; Robeson, L. M.; Elimelech, M.; Freeman, B. D. Maximizing the right stuff: The trade-off between membrane permeability and selectivity. *Science* **2017**, *356*, eaab0530.
(12) Abaie, E.; Xu, L.; Shen, Y.-x. Bioinspired and biomimetic membranes for water purification and chemical separation: A review. *Front. Environ. Sci. Eng.* **2021**, *15*, 124.
(13) Werber, J. R.; Osuji, C. O.; Elimelech, M. Materials for next-generation desalination and water purification membranes. *Nat. Rev. Mater.* **2016**, *1*, 16018.
(14) Huo, Y. P.; Zeng, H. Q. Sticky"-Ends-Guided Creation of Functional Hollow Nanopores for Guest Encapsulation and Water Transport. *Acc. Chem. Res.* **2016**, *49*, 922−930.
(15) Gong, B. Artificial water channels: inspiration, progress, and challenges. *Faraday Discuss.* **2018**, *209*, 415−427.
(16) Huang, L.-B.; Di Vincenzo, M.; Li, Y.; Barboiu, M. Artificial Water Channels: Towards Biomimetic Membranes for Desalination. *Chem.-Eur. J.* **2021**, *27*, 2224−2239.
(17) Percec, V.; Dulcey, A. E.; Balagurusamy, V. S. K.; Miura, Y.; Smidrkal, J.; Peterca, M.; Nummelin, S.; Edlund, U.; Hudson, S. D.; Heiney, P. A.; Duan, H.; Magonov, S. N.; Vinogradov, S. A. Self-assembly of amphiphilic dendritic dipeptides into helical pores. *Nature* **2004**, *430*, 764−768.
(18) Kaucher, M. S.; Peterca, M.; Dulcey, A. E.; Kim, A. J.; Vinogradov, S. A.; Hammer, D. A.; Heiney, P. A.; Percec, V. Selective Transport of Water Mediated by Porous Dendritic Dipeptides. *J. Am. Chem. Soc.* **2007**, *129*, 11698−11699.
(19) Le Duc, Y.; Michau, M.; Gilles, A.; Gence, V.; Legrand, Y.-M.; van der Lee, A.; Tingry, S.; Barboiu, M. Imidazole-Quartet Water and Proton Dipolar Channels. *Angew. Chem., Int. Ed.* **2011**, *50*, 11366−11372.
(20) Licsandru, E.; Kocsis, I.; Shen, Y.-x.; Murail, S.; Legrand, Y.-M.; van der Lee, A.; Tsai, D.; Baaden, M.; Kumar, M.; Barboiu, M. Salt-Excluding Artificial Water Channels Exhibiting Enhanced Dipolar Water and Proton Translocation. *J. Am. Chem. Soc.* **2016**, *138*, 5403−5409.
(21) Kocsis, I.; Sorci, M.; Vanselous, H.; Murail, S.; Sanders, S. E.; Licsandru, E.; Legrand, Y.-M.; van der Lee, A.; Baaden, M.; Petersen, P. B.; Belfort, G.; Barboiu, M. Oriented chiral water wires in artificial transmembrane channels. *Sci. Adv.* **2018**, *4*, No. eaao5603.
(22) Di Vincenzo, M.; Tiraferri, A.; Musteata, V.-E.; Chisca, S.; Sougrat, R.; Huang, L.-B.; Nunes, S. P.; Barboiu, M. Biomimetic artificial water channel membranes for enhanced desalination. *Nat. Nanotechnol.* **2021**, *16*, 190−196.
(23) Di Vincenzo, M.; Tiraferri, A.; Musteata, V.-E.; Chisca, S.; Deleanu, M.; Ricceri, F.; Cot, D.; Nunes, S. P.; Barboiu, M. Tunable membranes incorporating artificial water channels for high-performance brackish/low-salinity water reverse osmosis desalination. *Proc. Natl. Acad. Sci. U. S. A.* **2021**, *118*, No. e2022200118.
(24) Huang, L.-B.; Di Vincenzo, M.; Ahunbay, M. G.; van der Lee, A.; Cot, D.; Cerneaux, S.; Maurin, G.; Barboiu, M. Bilayer versus Polymeric Artificial Water Channel Membranes: Structural Determinants for Enhanced Filtration Performances. *J. Am. Chem. Soc.* **2021**, *143*, 14386−14393.
(25) Hu, X.-B.; Chen, Z.; Tang, G.; Hou, J.-L.; Li, Z.-T. Single-Molecular Artificial Transmembrane Water Channels. *J. Am. Chem. Soc.* **2012**, *134*, 8384−8387.
(26) Shen, Y.-x.; Si, W.; Erbakan, M.; Decker, K.; De Zorzi, R.; Saboe, P. O.; Kang, Y. J.; Majd, S.; Butler, P. J.; Walz, T.; Aksimentiev, A.; Hou, J.-l.; Kumar, M. Highly permeable artificial water channels that can self-assemble into two-dimensional arrays. *Proc. Natl. Acad. Sci. U.S.A.* **2015**, *112*, 9810.
(27) Yan, Z.-J.; Wang, D.; Ye, Z.; Fan, T.; Wu, G.; Deng, L.; Yang, L.; Li, B.; Liu, J.; Ma, T.; Dong, C.; Li, Z.-T.; Xiao, L.; Wang, Y.; Wang, W.; Hou, J.-L. Artificial Aquaporin That Restores Wound Healing of Impaired Cells. *J. Am. Chem. Soc.* **2020**, *142*, 15638−15643.
(28) Strilets, D.; Fa, S.; Hardiagon, A.; Baaden, M.; Ogoshi, T.; Barboiu, M. Biomimetic Approach for Highly Selective Artificial Water Channels Based on Tubular Pillar[5]arene Dimers. *Angew. Chem., Int. Ed.* **2020**, *59*, 23213−23219.
(29) Zhou, X.; Liu, G.; Yamato, K.; Shen, Y.; Cheng, R.; Wei, X.; Bai, W.; Gao, Y.; Li, H.; Liu, Y.; Liu, F.; Czajkowsky, D. M.; Wang, J.; Dabney, M. J.; Cai, Z.; Hu, J.; Bright, F. V.; He, L.; Zeng, X. C.; Shao, Z.; Gong, B. Self-assembling subnanometer pores with unusual mass-transport properties. *Nat. Commun.* **2012**, *3*, 949.
(30) Tunuguntla, R. H.; Allen, F. I.; Kim, K.; Belliveau, A.; Noy, A. Ultrafast proton transport in sub-1-nm diameter carbon nanotube porins. *Nat. Nanotechnol.* **2016**, *11*, 639−644.
(31) Tunuguntla, R. H.; Henley, R. Y.; Yao, Y.-C.; Pham, T. A.; Wanunu, M.; Noy, A. Enhanced water permeability and tunable ion selectivity in subnanometer carbon nanotube porins. *Science* **2017**, *357*, 792−796.
(32) Yuan, Y. D.; Dong, J.; Liu, J.; Zhao, D.; Wu, H.; Zhou, W.; Gan, H. X.; Tong, Y. W.; Jiang, J.; Zhao, D. Porous organic cages as synthetic water channels. *Nat. Commun.* **2020**, *11*, 4927.
(33) Shen, J.; Fan, J.; Ye, R. J.; Li, N.; Mu, Y.; Zeng, H. Q. Polypyridine-Based Helical Amide Foldamer Channels: Rapid Transport of Water and Protons with High Ion Rejection. *Angew. Chem., Int. Ed.* **2020**, *59*, 13328−13334.
(34) Shen, J.; Ye, R. J.; Romanies, A.; Roy, A.; Chen, F.; Ren, C. L.; Liu, Z.; Zeng, H. Q. Aquafoldmer-Based Aquaporin-like Synthetic Water Channel. *J. Am. Chem. Soc.* **2020**, *142*, 10050−10058.
(35) Roy, A.; Shen, J.; Joshi, H.; Song, W.; Tu, Y.-M.; Chowdhury, R.; Ye, R. J.; Li, N.; Ren, C.; Kumar, M.; Aksimentiev, A.; Zeng, H. Q. Foldamer-based ultrapermeable and highly selective artificial water channels that exclude protons. *Nat. Nanotechnol.* **2021**, *16*, 911−917.
(36) Huang, L.-B.; Hardiagon, A.; Kocsis, I.; Jegu, C.-A.; Deleanu, M.; Gilles, A.; van der Lee, A.; Sterpone, F.; Baaden, M.; Barboiu, M. Hydroxy Channels-Adaptive Pathways for Selective Water Cluster Permeation. *J. Am. Chem. Soc.* **2021**, *143*, 4224−4233.
(37) O'Hagan, D. Understanding organofluorine chemistry. An introduction to the C-F bond. *Chem. Soc. Rev.* **2008**, *37*, 308−319.
(38) Ren, C.; Zhou, F.; Qin, B.; Ye, R.; Shen, S.; Su, H.; Zeng, H. Q. Crystallographic Realization of the Mathematically Predicted Densest All-Pentagon Packing Lattice by C5-Symmetric "Sticky" Fluoropentamers. *Angew. Chem., Int. Ed.* **2011**, *50*, 10612−10615.
(39) Gan, Q.; Bao, C.; Kauffmann, B.; Grélard, A.; Xiang, J.; Liu, S.; Huc, I.; Jiang, H. Quadruple and Double Helices of 8-Fluoroquinoline Oligoamides. *Angew. Chem., Int. Ed.* **2008**, *47*, 1715−1718.
(40) Li, C.; Ren, S.-F.; Hou, J.-L.; Yi, H.-P.; Zhu, S.-Z.; Jiang, X.-K.; Li, Z.-T. F···H-N Hydrogen Bonding Driven Foldamers: Efficient Receptors for Dialkylammonium Ions. *Angew. Chem., Int. Ed.* **2005**, *44*, 5725−5729.
(41) Roy, A.; Joshi, H.; Ye, R.; Shen, J.; Chen, F.; Aksimentiev, A.; Zeng, H. Q. Polyhydrazide-Based Organic Nanotubes as Efficient and Selective Artificial Iodide Channels. *Angew. Chem., Int. Ed.* **2020**, *59*, 4806−4813.
(42) Mishra, S. K.; Suryaprakash, N. Intramolecular hydrogen bonds involving organic fluorine in the derivatives of hydrazides: an NMR

https://doi.org/10.1021/acs.nanolett.2c01137
Nano Lett. 2022, 22, 4831−4838

investigation substantiated by DFT based theoretical calculations. *Phys. Chem. Chem. Phys.* **2015**, *17*, 15226−15235.
(43) Yan, Y.; Qin, B.; Ren, C. L.; Chen, X. Y.; Yip, Y. K.; Ye, R. J.; Zhang, D. W.; Su, H. B.; Zeng, H. Q. Synthesis, structural investigations, hydrogen-deuterium exchange studies, and molecular modeling of conformationally stablilized aromatic oligoamides. *J. Am. Chem. Soc.* **2010**, *132*, 5869−5879.
(44) Ong, W. Q.; Zhao, H. Q.; Du, Z. Y.; Yeh, J. Z. Y.; Ren, C. L.; Tan, L. Z. W.; Zhang, K.; Zeng, H. Q. Computational prediction and experimental verification of pyridine-based helical oligoamides containing four repeating units per turn. *Chem. Commun.* **2011**, *47*, 6416−6418.
(45) Zhao, H. Q.; Ong, W. Q.; Fang, X.; Zhou, F.; Hii, M. N.; Li, S. F. Y.; Su, H. B.; Zeng, H. Q. Synthesis, Structural Investigation and Computational Modelling of Water-Binding Aquafoldamers. *Org. Biomol. Chem.* **2012**, *10*, 1172−1180.
(46) Guo, Y.; Pogodin, S.; Baulin, V. A. General model of phospholipid bilayers in fluid phase within the single chain mean field theory. *J. Chem. Phys.* **2014**, *140*, 174903.
(47) Hannesschläger, C.; Barta, T.; Siligan, C.; Horner, A. Quantification of Water Flux in Vesicular Systems. *Sci. Rep.* **2018**, *8*, 8516.
(48) Ren, C.; Ding, X.; Roy, A.; Shen, J.; Zhou, S.; Chen, F.; Yau Li, S. F.; Ren, H.; Yang, Y. Y.; Zeng, H. Q. A halogen bond-mediated highly active artificial chloride channel with high anticancer activity. *Chem. Sci.* **2018**, *9*, 4044−4051.
(49) Song, W.; Joshi, H.; Chowdhury, R.; Najem, J. S.; Shen, Y.-x.; Lang, C.; Henderson, C. B.; Tu, Y.-M.; Farell, M.; Pitz, M. E.; Maranas, C. D.; Cremer, P. S.; Hickey, R. J.; Sarles, S. A.; Hou, J.-l.; Aksimentiev, A.; Kumar, M. Artificial water channels enable fast and selective water permeation through water-wire networks. *Nat. Nanotechnol.* **2020**, *15*, 73−79.
(50) Werber, J. R.; Elimelech, M. Permselectivity limits of biomimetic desalination membranes. *Sci. Adv.* **2018**, *4*, No. eaar8266.
(51) Song, W.; Kumar, M. Artificial water channels: toward and beyond desalination. *Curr. Opin. Chem. Eng.* **2019**, *25*, 9−17.
(52) Kosinska Eriksson, U.; Fischer, G.; Friemann, R.; Enkavi, G.; Tajkhorshid, E.; Neutze, R. Subangstrom Resolution X-Ray Structure Details Aquaporin-Water Interactions. *Science* **2013**, *340*, 1346−1349.
(53) Zhang, C.; Wu, J.; Galli, G.; Gygi, F. Structural and Vibrational Properties of Liquid Water from van der Waals Density Functionals. *J. Chem. Theory Comput.* **2011**, *7*, 3054−3061.
(54) Li, Y.; Li, Z.; Aydin, F.; Quan, J.; Chen, X.; Yao, Y.-C.; Zhan, C.; Chen, Y.; Pham, T. A.; Noy, A. Water-ion permselectivity of narrow-diameter carbon nanotubes. *Sci. Adv.* **2020**, *6*, No. eaba9966.
(55) Freger, V. Selectivity and polarization in water channel membranes: lessons learned from polymeric membranes and CNTs. *Faraday Discuss.* **2018**, *209*, 371−388.
(56) Pohl, P.; Saparov, S. M.; Borgnia, M. J.; Agre, P. Highly selective water channel activity measured by voltage clamp: Analysis of planar lipid bilayers reconstituted with purified AqpZ. *Proc. Natl. Acad. Sci. U.S.A.* **2001**, *98*, 9624−9629.

https://doi.org/10.1021/acs.nanolett.2c01137
Nano Lett. 2022, 22, 4831−4838